Journal of Electrical Engineering & Technology (2020) 15:2057–2077
https://doi.org/10.1007/s42835-020-00499-2

ORIGINAL ARTICLE

# Analysis of the Effects of PSS and Renewable Integration to an Inter-Area Power Network to Improve Small Signal Stability

Prasenjit Dey[1] · Anulekha Saha[1] · Aniruddha Bhattacharya[2] · Boonruang Marungsri[3]

Received: 16 December 2019 / Revised: 24 May 2020 / Accepted: 28 July 2020 / Published online: 3 August 2020


## Abstract
Power system often suffers from low frequency oscillations (LFOs) which might result in instability in the long run, if allowed to sustain in the system for a long time. In order to mitigate these oscillations, power system stabilizers (PSS) are used through excitation control. Three recently developed meta-heuristic algorithms namely: Collective Decision Optimization (CDO), Grasshopper Optimization Algorithm (GOA) and Salp Swarm Algorithm (SSA) have been applied for the optimal tuning of PSS parameters for small signal stability analysis of a renewable integrated power network. This was done by designing a conventional speed-based lead-lag PSS in a multi-machine interconnected power system, whose parameters have been tuned using CDO, GOA and SSA in a way to shift all the eigenvalues associated to electromechanical modes to the left half of S plane. Comparison of the results obtained by the algorithms demonstrates the superiority of SSA over GOA and CDO to boost the overall system stability over a wide range of operating conditions. The PSS controller designed using SSA is observed to be more robust and efficient in damping out oscillations under different operating conditions.

**Keywords** Eigenvalues · Multi-machine power system · Power system stabilizer · Salp swarm algorithm

## Abbreviations

| | |
|---|---|
| PSSs | Power system stabilizers |
| CDO | Collective Decision Optimization |
| GOA | Grasshopper Optimization Algorithm |
| SSA | Salp Swarm Algorithm |
| PLL | Phase Locked Loop |
| MPPT | Maximum Power Point Tracking |
| LFOs | Low frequency oscillations |
| LTI | Linear time-invariant |
| $R_S$ and $R_P$ | Parasitic resistance |
| D | Duty ratio |
| $\Delta\omega$ | Angular Frequency Deviation |
| $\delta$ | Rotor Electrical Angular Position |
| $P_e$ | Output electrical power |
| $i_{fd}$ | Field current |
| $V_t$ | Generator terminal voltage |
| $X'_d$ | Direct axis transient reactance |
| $R_f$ | Rate feedback |
| $E'_d$ | Direct axis component of voltage behind $X'_q$ |
| $T_A$ | Voltage regulator time constant |
| $T_2$ and $T_4$ | Phase-lag time constants |
| $GH$ | Grasshopper |
| $LD$ | Leaders |
| $FL$ | Followers |
| $ub$ | Upper bound |
| $lb$ | Lower bound |
| DAE | Differential algebraic equations |
| SSSA | Small signal stability analysis |
| PV | Photovoltaic |
| G | Solar irradiation |
| $\Delta I_L$ | Ripple current |
| $T_w$ | Time constant of washout filter |
| $E_{fd}$ | Field voltage |
| $H$ | Inertia constant of the generator |
| $T'_{d0}$ | Short circuit direct axis transient time constant |
| $X_d$ | Direct axis synchronous reactance |
| $X'_q$ | Quadrature axis transient reactance |
| $T_M$ | Mechanical torque to the shaft |

✉ Prasenjit Dey
deyprasenjit87@gmail.com

[1] Electrical and Electronics Engineering Department, National Institute of Technology Sikkim, Ravangla, Sikkim 737139, India

[2] Electrical Engineering Department, National Institute of Technology Durgapur, Durgapur, West Bengal 713209, India

[3] School of Electrical Engineering, Suranaree University of Technology, Nakhon Ratchasima 30000, Thailand

| | |
|---|---|
| $S_E(E_{fd})$ | Saturation function |
| $K_{PSS}$ | Power system stabilizer gain |
| $J$ | Objective function |
| WSCC | Western system coordinating council |
| maxFE | Maximum fitness evaluation |
| FE | Fitness evaluation |
| SW | Swarm |
| EMs | Electromechanical modes |
| VSI | Voltage source inverter |
| STC | Standard temperature condition |
| SOFs | Sub-objective functions |
| L | Inductor |
| C | DC link capacitor |
| $\omega$ | Rotor electrical angular velocity |
| $P_m$ | Input mechanical power |
| $\xi$ | Damping ratio |
| $T'_{q0}$ | Short circuit quadrature axis transient time constant |
| $X_q$ | Quadrature axis synchronous reactance |
| $V_R$ | Output of Aaplifier |
| $E'_q$ | Quadrature axis component of voltage behind $X'_d$ |
| $K_A$ | Voltage regulator gain |
| $\sigma$ | Real part of eigenvalues |
| $T_1$ and $T_3$ | Phase-lead time constants |

## 1 Introduction

The electric utility industries have undergone exceptional changes in their structure worldwide. Newer issues in power system operation and planning are unavoidable due to the start of an open market environment and restructuring of the industries into distinct generation, transmission, and distribution entities. In this restructured power scenario, major emphasis is given on the delivery of stable, secure, controlled, and high quality electric power by the utilities. Power systems are broadly categorized into generation, transmission and distribution networks. During the transfer of electric power from generating station to consumer end, balance of both active and reactive power between the two ends is necessary. Active and reactive power relates to two equilibrium points: frequency and voltage. If either of the two balances is not maintained, the equilibrium points will float. A good quality electric power system signifies that there are no deviations in frequency and voltage from their desired values during operation. However, the main concern related to the system load is that, it is ever-changing based on the needs of the consumers which disrupts the active and reactive power balance. Due to the imbalance, the frequency and voltage levels will not be maintained to their standard values. Thus, a proper control system is essential to mitigate the effects of random load changes and to maintain the frequency and voltage at desired levels for maintaining stability of power system and ensure its reliable operation. Due to the presence of weak ties in a multi area network, power systems face frequency oscillations of varying degrees. These oscillations may sustain and grow which might eventually lead the system towards isolation. Therefore, the analysis of system stability is of utmost importance. Power system stability refers to the ability to remain in operating equilibrium. The power system becomes vulnerable to instability due to disturbances like sudden changes in load, loss of generation or switching of a transmission line during the fault, wide spread use of the high gain fast acting excitation system etc. In the past, stability was mainly categorized into angle stability and voltage stability. Angle stability can be further classified as: small signal stability, transient stability, mid-term stability and long-term stability. System stability depends on both damping and synchronizing torque components. Lack of sufficient synchronizing torque results in transient instability and insufficient damping torque results in small signal instability. Use of fast acting exciter models in modern power system helps in improving transient stability, but at the cost of damping torque, which makes the study of small signal stability an ultimate necessity. Small signal stability always deals with LFOs, which limits the power transmission capability and might eventually result in a breakdown of the entire system. Therefore, small signal stability analysis (SSSA) [1] is of prime importance for stable and secure operation of power system. PSSs [2] are commonly effective in mitigating these oscillations. PSS is employed to provide the supplementary control signal for excitation system of the synchronous generator to damp out the low frequency oscillations and to improve overall power system stability. In literature, PSSs have been designed mostly using phase compensation techniques and the parameters of PSS have been optimized based on power system detailed model including network equations [3, 4]. Various classical techniques *LMI* [5, 6], Pole placement method [7] etc. are available in the literature which can provide good performance but are not capable of solving non-differential, complex non-convex objective functions. Therefore, for the modern complex and dynamic power system, it is difficult to solve LFO problem through conventional and linear optimal control approaches. For different loading conditions and configurations of power network, the PSS parameters need to be modified. To overcome the limitations of classical optimization techniques, different evolutionary algorithms have been proposed in various literatures [8–23]. Evolutionary algorithms have become very attractive nowadays because of their easy implementation and lesser computational time in achieving global optimal point over the classical techniques. Literature shows that PSS tuning is a very challenging task till date thereby motivating the authors in applying three recently developed algorithms for tuning of PSS parameters.

Although Genetic algorithm (GA) [24] gained huge attention for designing of PSS due to its ease of getting near global optimal solutions, its application is constrained by large computational time.

Other evolutionary computation algorithms available in literatures for designing Conventional PSS to mitigate low frequency oscillations are: Bacteria Foraging (BF) [23], which is based on random search directions, which may lead to delay in reaching optimum solution, Firefly algorithm (FA) [25], Cuckoo search (CS) [18], Evolutionary programming [19], Tabu search [20], Simulated annealing [21] and BAT [22] etc.

With the increasing growth of population and economy, the developed as well as developing countries are facing a huge demand of energy. Keeping in mind the climate changes and other ill effects of greenhouse gas emissions from fossil fuel combustions, fulfilling this ever- increasing energy demand is quite challenging. Also, since fossil fuels are not unlimited, research is going on to find other alternate and efficient energy sources.

Utilization of energy obtained from renewable energy sources such as wind [26], solar [27] and hydro [28] goes a long way in reducing carbon emissions. Renewable energy sources are cleaner and cheaper alternatives for fossil fuels. Presently, there is an increased emphasis on solar photovoltaic (PV) generators as renewable energy sources because of their certain advantages such as simplicity of allocation and absence of fuel cost. But it is very important to observe the impact of renewable integration into the system. The introduction of renewable energy resources has resulted in the introduction of newer types of generators into electricity distribution systems. These PV generators do not have rotating mechanical parts and the power injections from these generators are dependent on and solar irradiation [29]. Operating the renewable generators in parallel with conventional synchronous generators present new challenges related to stability, operation and control of the power system and its components [30]. Therefore, it is necessary to study the impact of renewable integration on the small signal stability of the system.

Different methods like frequency response, residue based technique, synchronizing and damping torque analysis and eigenvalue analysis are available for analyzing small signal stability. But among all the above mentioned techniques, eigenvalue analysis technique is used in this paper because using this technique the oscillations can be characterized very easily and accurately. Also, various modes identification can be done easily by this technique, which is quite difficult with the other techniques available in the literature. The main contributions of this paper are as follows:

- Small signal stability analysis of solar PV integrated multi-machine system due to the dynamic behavior of the power system in presence of PSS is presented in this paper. An exhaustive comparative study is carried out for this solar integrated system with respect to the conventional system to demonstrate the effect of renewables on power system stability.
- Studies presented in the literature analyzed small signal stability considering R, L, C as local loads in case of solar PV. But constant power, constant current and constant impedance loads are more realistic that also needs to be addressed. This work considered constant power load for modeling purposes.

Section 2 of the paper presents the techniques which are available for small signal stability analysis; brief description of electromechanical modes and participation factor is presented in Sect. 3; mathematical modeling of power system stabilizer and solar PV integrated multi-machine model is presented in Sect. 4; objective function considered for the study and the optimization techniques applied are presented in Sects. 5 and 6 presents the results of simulation and their exhaustive discussion.

## 2 Small Signal Stability Analysis (SSSA)

The following are the commonly used techniques for small signal stability analysis:

2.1 Eigenvalue Technique [31]
2.2 Synchronizing and Damping Torque Analysis [2, 32]
2.3 Frequency Response and Residue Based Analysis [33–36]
2.4 Time Domain Solution [36–38]

The eigenvalue technique used in this paper is briefly described below:

Eigenvalues of any matrix $A$ are the results of the characteristic equation of the matrix, which may be real or complex. Complex eigenvalues always appear in conjugate pairs. For any eigenvalue $\lambda_i$, the time dependent characteristic of its mode is obtained as $e^{\lambda_i t}$ [31]. A real eigenvalue relates to a non-oscillatory mode. A positive real eigenvalue signifies aperiodic monotonic instability while negative real eigenvalue signifies a decaying mode. Higher the magnitude, faster is the decay. Each complex eigenvalue pair relates to an oscillatory mode. The real part of eigenvalue is associated to damping whereas; the imaginary part is associated to frequency of oscillations. A negative real part signifies damped oscillations while positive real part signifies oscillations with increasing amplitude. A complex pair of eigenvalues is represented as follows:

$$\lambda = \sigma \pm j\omega \tag{1}$$

The frequency of oscillation is obtained as: $f = \frac{\omega}{2\pi}$ and the damping ratio is obtained as:

$$\xi = \frac{\sigma}{\sqrt{\sigma^2 + \omega^2}} \tag{2}$$

The damping ratio $\xi$ helps to determine the rate of decay of the amplitude of oscillation. For a power system to perform stable operation, it needs to be ensured that real parts of all eigenvalues lie in the negative half of s-plane. Further, quick damping of any electromechanical oscillation should be ensured.

## 3 Identifying Electromechanical Modes (EMs) and Participation Factor (PF)

Small Signal Stability analysis is performed on the linearized dynamic model of the multi-machine system. In this analysis, the target is to study the low-frequency oscillations. Here, the interest lies particularly in the electromechanical modes (EMs). The electromechanical oscillations are of two types:

- Local mode: typical range of oscillation is 0.8–2.5 Hz.
- Inter-area mode: range of oscillation is 0.2–0.8 Hz.

In order to determine the significant participation of a machine in the EMs, the participation factor analysis is used. Participation factor analysis helps in the identification of how each state variable affects a given mode or eigenvalue [1].

## 4 Mathematical Modeling

### 4.1 Description of Power System Model

The small-perturbation behavior of the power system in the vicinity of a steady-state operating point can be described by a set of linear time-invariant (LTI) differential equation in the state space form as,

$$\dot{X} = AX + BU \tag{3}$$

where, perturbations of the system state variables from their nominal values at a given operating condition is represented by the $N$-dimensional state vector $X$, and perturbations of the system inputs such as voltage reference, desired real power or load demands is represented by the vector $U$. The numerical values of the matrices $A$ and $B$ depend on the operating condition as well as on the system parameters. The whole analysis starts with a systematic derivation of a linear model for an $n$-bus $m$-machine system with nonlinear voltage-dependent loads at the network buses.

In [1] the generator differential equations, stator algebraic equation and the network equations have been shown for two-axis model with Type I exciter. Next, after performing the load flow and computing the initial condition values of the state and algebraic variables, these equations have to be linearized in order to form the system matrix and calculate the eigenvalues of the system. The equations can be written in a generalized form as:

$$\left.\begin{aligned} \dot{x} &= f(x, y, u) \\ 0 &= g(x, y) \end{aligned}\right\} \tag{4}$$

Equation (4) consists of the stator algebraic equations and differential equations, together with the network equations. The state vector is denoted by $x$, the input vector is denoted by $u$, and $y$ includes both $I_{d\_q}$ and $\overline{V}$ vectors i.e.

$$y = \left[ I_{d-q}^t \ \theta_1 \ V_1 \ldots V_m \mid \theta_2 \ldots \theta_n \ V_{m+1} \ldots V_n \right]^t \left[ y_a^t \mid y_b^t \right]^t \tag{5}$$

Here, vector $y_b$ and $y_a$ corresponds to the load-flow variables and algebraic variables $I_{d-q}$ respectively. Bus 1 is the slack bus, buses 2,….,$m$ are the PV buses and buses $m+1$, …, $n$ are the $PQ$ buses. The vector $x$ has a dimension of $7m$. Linearizing (4) around an operating point we get:

$$\begin{bmatrix} \frac{d}{dt}\Delta x \\ 0 \\ 0 \end{bmatrix} = \begin{bmatrix} A & \multicolumn{2}{c}{B} \\ C & D_{11} & D_{12} \\ & D_{21} & D_{22} \end{bmatrix} \begin{bmatrix} \Delta x \\ \Delta y_a \\ \Delta y_b \end{bmatrix} + E[\Delta u] \tag{6}$$

By eliminating $\Delta y_a$ and $\Delta y_b$, we get $\Delta \dot{x} = A_{sys}\Delta x$ where $A_{sys} = \left(A - BJ_{AE}^{-1}C\right)$ where $J_{AE} = \begin{bmatrix} D_{11} & D_{12} \\ D_{21} & D_{22} \end{bmatrix}$.

The model represented using (6) has been used for the small signal stability analysis in this work. The linearized differential equations, stator algebraic equations and network equation are presented below [39].

#### 4.1.1 Linearized Differential Equations

$$\frac{d\Delta\delta_i}{dt} = \Delta\omega_i \tag{7}$$

$$\frac{d\Delta\omega_i}{dt}=-\frac{D_i}{M_i}\Delta\omega_i-\frac{I_{qio}}{M_i}\Delta E'_{qi}-\frac{I_{dio}}{M_i}\Delta E'_{di}-\frac{I_{qio}\left(X'_{qi}-X'_{di}\right)+E'_{dio}}{M_i}\Delta I_{di}$$
$$-\frac{I_{dio}\left(X'_{qi}-X'_{di}\right)+E'_{qio}}{M_i}\Delta I_{qi}+\frac{1}{M_i}\Delta T_{Mi} \tag{8}$$

$$\frac{d\Delta E'_{qi}}{dt}=-\frac{1}{T'_{doi}}\Delta E'_{qi}+\frac{1}{T'_{doi}}\Delta E_{fdi}-\frac{\left(X_{di}-X'_{di}\right)}{T'_{doi}}\Delta I_{di} \tag{9}$$

$$\frac{d\Delta E'_{di}}{dt}=-\frac{1}{T'_{qoi}}\Delta E'_{di}+\frac{\left(X_{qi}-X'_{qi}\right)}{T'_{qoi}}\Delta I_{qi} \tag{10}$$

$$\frac{d\Delta E_{fdi}}{dt}=f_{si}\left(E_{fdio}\right)+\frac{1}{T_{Ei}}\Delta V_{Ri} \tag{11}$$

where $f_{si}\left(E_{fdio}\right)=-\frac{1}{T_{Ei}}\left(K_{Ei}+S_E\left(E_{fdi}\right)+E_{fdio}\delta S_E\left(E_{fdi}\right)\right)$; and $S_E\left(E_{fdi}\right)=0.0039e^{1.555E_{fdi}}$

$$\frac{d\Delta V_{Ri}}{dt}=-\frac{K_{Ai}K_{Fi}}{T_{Ai}T_{Fi}}\Delta E_{fdi}-\frac{1}{T_{Ai}}\Delta V_{Ri}+\frac{K_{Ai}}{T_{Ai}}\Delta R_{fi}+\frac{K_{Ai}}{T_{Ai}}\Delta V_{refi}-\frac{K_{Ai}}{T_{Ai}}\Delta V_i \tag{12}$$

$$\frac{d\Delta R_{Fi}}{dt}=-\frac{1}{T_{Fi}}\Delta R_{Fi}+\frac{K_{Fi}}{\left(T_{Fi}\right)^2}\Delta E_{fdi} \tag{13}$$

For $i=1, 2,\ldots, m$,

#### 4.1.2 Linearized Stator Algebraic Equations

$$\Delta E'_{di}-\sin\left(\delta_{io}-\theta_{io}\right)\Delta V_i-V_{io}\cos\left(\delta_{io}-\theta_{io}\right)\Delta\delta_i+V_{io}\cos\left(\delta_{io}-\theta_{io}\right)\Delta\theta_i-R_{si}\Delta I_{di}+X'_{qi}\Delta I_{qi}=0 \tag{14}$$

$$\Delta E'_{qi}-\cos\left(\delta_{io}-\theta_{io}\right)\Delta V_i+V_{io}\sin\left(\delta_{io}-\theta_{io}\right)\Delta\delta_i-V_{io}\sin\left(\delta_{io}-\theta_{io}\right)\Delta\theta_i-R_{si}\Delta I_{qi}-X'_{di}\Delta I_{di}=0 \tag{15}$$

#### 4.1.3 Linearized Network Equations

Similarly, linearizing the network equations for load buses, we get [39]

$$\begin{aligned}&I_{dio}V_{io}\cos\left(\delta_{io}-\theta_{io}\right)\Delta\delta_i-I_{qio}V_{io}\sin\left(\delta_{io}-\theta_{io}\right)\Delta\delta_i+V_{io}\sin\left(\delta_{io}-\theta_{io}\right)\Delta I_{di}\\&\quad+V_{io}\cos\left(\delta_{io}-\theta_{io}\right)\Delta I_{qi}-I_{dio}V_{io}\cos\left(\delta_{io}-\theta_{io}\right)\Delta\theta_i+I_{qio}V_{io}\sin\left(\delta_{io}-\theta_{io}\right)\Delta\theta_i\\&\quad+V_{io}\sum_{k=1\neq i}^{n}V_{ko}Y_{ik}\sin\left(\theta_{io}-\theta_{ko}-\alpha_{ik}\right)\Delta\theta_i+I_{dio}\sin\left(\delta_{io}-\theta_{io}\right)\Delta V_i+\frac{\delta P_{Li}\left(V_i\right)}{\delta V_i}\Delta V_i\\&\quad-\sum_{k=1}^{n}V_{ko}Y_{ik}\cos\left(\theta_{io}-\theta_{ko}-\alpha_{ik}\right)\Delta V_i-V_{io}\sum_{k=1\neq i}^{n}V_{ko}Y_{ik}\sin\left(\theta_{io}-\theta_{ko}-\alpha_{ik}\right)\Delta\theta_k\\&\quad-V_{io}\sum_{k=1}^{n}Y_{ik}\cos\left(\theta_{io}-\theta_{ko}-\alpha_{ik}\right)\Delta V_k+I_{qio}\cos\left(\delta_{io}-\theta_{io}\right)\Delta V_{ik}=0\end{aligned} \tag{16}$$

$$\begin{aligned}&-I_{dio}V_{io}\sin\left(\delta_{io}-\theta_{io}\right)\Delta\delta_i-I_{qio}V_{io}\cos\left(\delta_{io}-\theta_{io}\right)\Delta\delta_i+V_{io}\cos\left(\delta_{io}-\theta_{io}\right)\Delta I_{di}\\&-V_{io}\sin\left(\delta_{io}-\theta_{io}\right)\Delta I_{qi}+I_{dio}V_{io}\sin\left(\delta_{io}-\theta_{io}\right)\Delta\theta_i+I_{qio}V_{io}\cos\left(\delta_{io}-\theta_{io}\right)\Delta\theta_i\\&-V_{io}\sum_{k=1\neq i}^{n}V_{ko}Y_{ik}\cos\left(\theta_{io}-\theta_{ko}-\alpha_{ik}\right)\Delta\theta_i+I_{dio}\cos\left(\delta_{io}-\theta_{io}\right)\Delta V_i+\frac{\delta Q_{Li}\left(V_i\right)}{\delta V_i}\Delta V_i\\&-\sum_{k=1}^{n}V_{ko}Y_{ik}\sin\left(\theta_{io}-\theta_{ko}-\alpha_{ik}\right)\Delta V_i+V_{io}\sum_{k=1\neq i}^{n}V_{ko}Y_{ik}\cos\left(\theta_{io}-\theta_{ko}-\alpha_{ik}\right)\Delta\theta_k\\&-V_{io}\sum_{k=1}^{n}Y_{ik}\sin\left(\theta_{io}-\theta_{ko}-\alpha_{ik}\right)\Delta V_k-I_{qio}\sin\left(\delta_{io}-\theta_{io}\right)\Delta V_{ik}=0\end{aligned} \tag{17}$$

Now linearizing the network equations for load buses

$$\sum_{\substack{k=1\\ \neq i}}^{n} V_{io}V_{ko}Y_{ik}\sin\left(\theta_{io}-\theta_k-\alpha_{ik}\right)\Delta\theta_i+\frac{\delta P_{Li}\left(V_i\right)}{\delta V_i}\Delta V_i$$
$$-\sum_{k=1}^{n} V_{ko}Y_{ik}\cos\left(\theta_{io}-\theta_k-\alpha_{ik}\right)\Delta V_i$$
$$-V_{io}\sum_{\substack{k=1\\ \neq i}}^{n} V_{ko}Y_{ik}\sin\left(\theta_{io}-\theta_{ko}-\alpha_{ik}\right)\Delta\theta_k$$
$$-V_{io}\sum_{k=1}^{n} Y_{ik}\cos\left(\theta_{io}-\theta_k-\alpha_{ik}\right)\Delta V_k=0 \tag{18}$$

$$-\sum_{\substack{k=1\\ \neq i}}^{n} V_{io}V_{ko}Y_{ik}\cos\left(\theta_{io}-\theta_k-\alpha_{ik}\right)\Delta\theta_i+\frac{\delta Q_{Li}\left(V_i\right)}{\delta V_i}\Delta V_i$$
$$-\sum_{k=1}^{n} V_{ko}Y_{ik}\sin\left(\theta_{io}-\theta_k-\alpha_{ik}\right)\Delta V_i$$
$$+V_{io}\sum_{\substack{k=1\\ \neq i}}^{n} V_{ko}Y_{ik}\cos\left(\theta_{io}-\theta_{ko}-\alpha_{ik}\right)\Delta\theta_k$$
$$-V_{io}\sum_{k=1}^{n} Y_{ik}\sin\left(\theta_{io}-\theta_k-\alpha_{ik}\right)\Delta V_k=0 \tag{19}$$

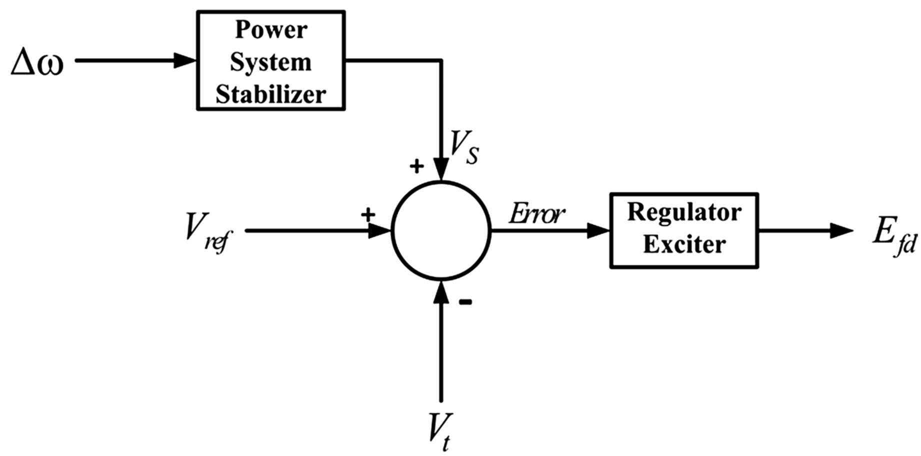


**Fig. 1** Schematic diagram of the stabilizing signal from speed deviation

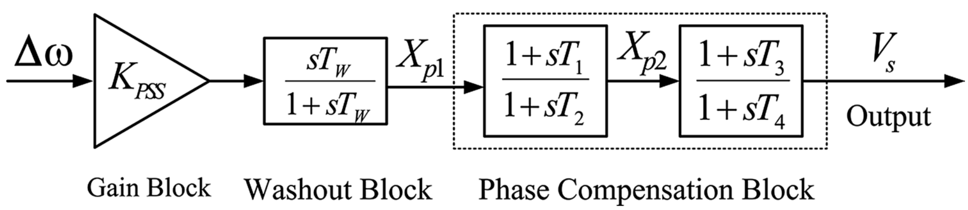


**Fig. 2** Block diagram of double-stage PSS [41]

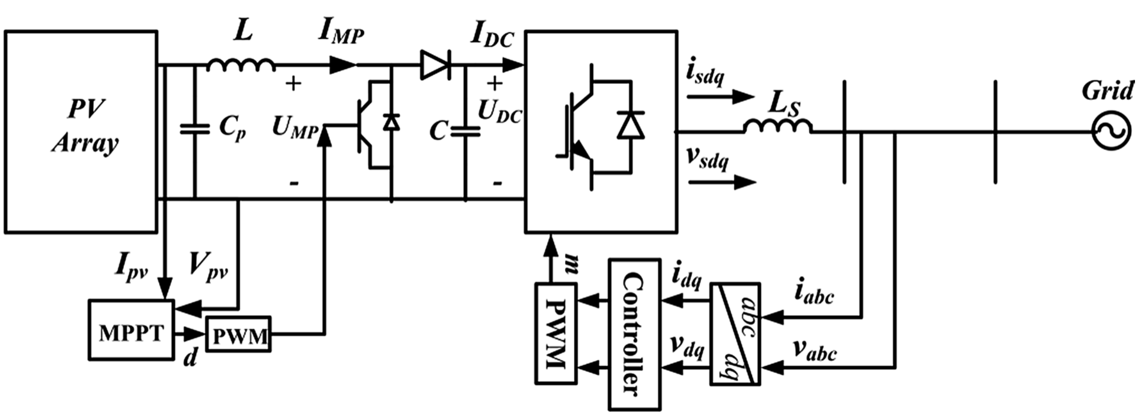


**Fig. 3** Single-line diagram of the grid connected PV system [42]

## 4.2 Power System Stabilizer

The main idea behind installation of the Power System Stabilizer (PSS) is to damp out system oscillations by providing additional damping to the synchronous machine by controlling its excitation using auxiliary stabilizing signal(s) [39].

### 4.2.1 Components of PSS

During periods of transient, it has been observed that the voltage regulator introduces negative damping to the system [40]. In order to counter this effect and to improve the overall system damping, artificial means of producing torque in phase with the speed deviation are introduced. Stabilizing signals are introduced to the excitation system at the summing junction where the reference voltage and the signal produced from the terminal voltage are added to obtain the error signal, which is fed to the regulator-exciter system. This has been shown in Fig. 1. The basic block diagram of the two-stage Power System Stabilizer is provided in Fig. 2.

It consists of four blocks: two phase compensation block, a signal washout filter block and a gain.

### 4.2.2 Modeling of Power System Stabilizer

From the block diagram of PSS is given in Fig. 2. The following linearized equations can be derived:

$$\Delta X_{p1} = \frac{sK_{PSS}T_w}{1 + sT_w}\Delta\omega_r \tag{20}$$

$$\Delta X_{p2} = \frac{1 + sT_1}{1 + sT_2}\Delta X_{p1} \tag{21}$$

$$\Delta V_s = \frac{1 + sT_3}{1 + sT_4}\Delta X_{p2} \tag{22}$$

where $\Delta\omega_r = \frac{\Delta\omega_i}{\omega_s}$ and $\omega_s$ is the synchronous speed.

From (8) of Sect. 4.1, we get the linearized expression of $\Delta\omega_i$ as:

$$\begin{aligned}\frac{d\Delta\omega_i}{dt} &= -\frac{D_i}{M_i}\Delta\omega_i - \frac{I_{qio}}{M_i}\Delta E'_{qi} - \frac{I_{dio}}{M_i}\Delta E'_{di} - \frac{I_{qio}\left(X'_{qi} - X'_{di}\right) + E'_{dio}}{M_i}\Delta I_{di}\\ &-\frac{I_{dio}\left(X'_{qi} - X'_{di}\right) + E'_{qio}}{M_i}\Delta I_{qi} + \frac{1}{M_i}\Delta T_{Mi}\end{aligned} \tag{23}$$

Using (20)–(22), the linearized model of the PSS model is obtained, and state equations of PSS are given below:

$$\begin{aligned}\Delta\dot{X}_{p1i} &= -\frac{K_{PSSi}D_i}{\omega_s M_i}\Delta\omega_i - \frac{K_{PSSi}I_{qio}}{\omega_s M_i}\Delta E'_{qi} - \frac{K_{PSSi}I_{dio}}{\omega_s M_i}\Delta E'_{di}\\ &+\frac{K_{PSSi}\left\{\left(X'_{di} - X'_{qi}\right)I_{qio} - E'_{dio}\right\}}{\omega_s M_i}\Delta I_{dio} + \frac{K_{PSSi}\left\{\left(X'_{di} - X'_{qi}\right)I_{dio} - E'_{qio}\right\}}{\omega_s M_i}\Delta I_{qio}\\ &-\frac{1}{T_w}\Delta X_{p1i} + \frac{K_{PSSi}}{\omega_s M_i}\Delta T_{Mi}\end{aligned} \tag{24}$$

$$\begin{aligned}\Delta\dot{X}_{p2i} &= -\frac{K_{PSSi}D_iT_{1i}}{\omega_s M_iT_{2i}}\Delta\omega_i - \frac{K_{PSSi}I_{qio}T_{1i}}{\omega_s M_iT_{2i}}\Delta E'_{qi} - \frac{K_{PSS}I_{dio}T_{1i}}{\omega_s M_iT_{2i}}\Delta E'_{di}\\ &+\frac{K_{PSS}T_{1i}\left\{\left(X'_{di} - X'_{qi}\right)I_{qio} - E'_{dio}\right\}}{\omega_s M_iT_{2i}}\Delta I_{dio} + \frac{K_{PSS}T_{1i}\left\{\left(X'_{di} - X'_{qi}\right)I_{dio} - E'_{qio}\right\}}{\omega_s M_iT_{2i}}\Delta I_{qio}\\ &+\frac{1}{T_{2i}}\left(1 - \frac{T_{1i}}{T_w}\right)\Delta X_{p1i} - \frac{1}{T_{2i}}\Delta X_{p2i} + \frac{K_{PSS}T_{1i}}{\omega_s M_iT_{2i}}\Delta T_{Mi}\end{aligned} \tag{25}$$

$$\Delta\dot{V}_{si}=-\frac{K_{PSSi}D_iT_{1i}T_{3i}}{\omega_sM_iT_{2i}T_{4i}}\Delta\omega_i-\frac{K_{PSSi}I_{qio}T_{1i}T_{3i}}{\omega_sM_iT_{2i}T_{4i}}\Delta E'_{qi}-\frac{K_{PSS}I_{dio}T_{1i}T_{3i}}{\omega_sM_iT_{2i}T_{4i}}\Delta E'_{di}$$
$$+\frac{K_{PSS}T_{1i}T_{3i}\left\{\left(X'_{di}-X'_{qi}\right)I_{qio}-E'_{dio}\right\}}{\omega_sM_iT_{2i}T_{4i}}\Delta I_{dio}+\frac{K_{PSS}T_{1i}T_{3i}\left\{\left(X'_{di}-X'_{qi}\right)I_{dio}-E'_{qio}\right\}}{\omega_sM_iT_{2i}T_{4i}}\Delta I_{qio} \tag{26}$$
$$+\frac{T_{3i}}{T_{2i}T_{4i}}\left(1-\frac{T_{1i}}{T_w}\right)\Delta X_{p1i}+\frac{1}{T_{4i}}\left(1-\frac{T_{3i}}{T_{2i}}\right)\Delta X_{p2i}-\frac{1}{T_{4i}}\Delta V_{si}+\frac{K_{PSS}T_{3i}}{\omega_sM_iT_{4i}}\Delta T_{Mi}$$

### 4.3 SSSA for Grid Connected Solar Photovoltaic

Grid connected Photovoltaic (PV) systems that are connected to the distribution level, particularly with MW capacity, are increasing at an aggressive rate, in order to meet the energy demand. However, there is less experience in the interconnection of utility-scale PV systems with the distribution network, where loads are present. Also, there has been very less work and research in interconnection of large-scale PV system with the transmission network for generation of bulk electric power. Utility-scale PV systems need special attention, unlike small scale PV systems, which are limited to a few hundreds of kW and are unlikely to show an impression on the transmission system. Thus, there is a need to analyze the large-scale PV systems in terms of dynamic characteristics and stability.

#### 4.3.1 Linearized System Model with Solar Integration

A single-line diagram for grid-connected PV system is shown in Fig. 3:

The solar PV system along with its components, has been modeled and can be represented by the following differential equations [42]:

$$L\dot{i}_{mp}=v_{mp}-Dv_{DC} \tag{27}$$

$$C\dot{v}_{DC}=Di_{mp}-i_{DC} \tag{28}$$

$$v_{sd}=v_d-\omega_{PLL}L_Si_q+L_s\dot{i}_d \tag{29}$$

$$v_{sq}=v_q+\omega_{PLL}L_Si_d+L_s\dot{i}_q \tag{30}$$

$$\dot{v}_{sd}-k_{ii}i_{dref}+k_{ii}i_d+\omega_{PLL}v_{sq}-\omega_{PLL}v_q-\omega_{PLL}^2L_Si_d=0 \tag{31}$$

$$\dot{v}_{sq}-k_{ii}i_{qref}+k_{ii}i_q-\omega_{PLL}v_{sd}+\omega_{PLL}v_d-\omega_{PLL}^2L_Si_d=0 \tag{32}$$

and, by the power balance equation:

$$v_{DC}i_{DC}=v_{sd}i_d+v_{sq}i_q \tag{33}$$

Linearizing (27)–(33), we get

$$\Delta\dot{i}_{mp}=\frac{1}{L}\Delta v_{mp}-\frac{D_0}{L}\Delta v_{DC} \tag{34}$$

$$\Delta\dot{v}_{DC}=\frac{D_0}{C}\Delta i_{mp} \tag{35}$$

$$\Delta\dot{i}_d=\frac{1}{L_S}\Delta v_{sd}+\omega_{PLL0}\Delta i_q \tag{36}$$

$$\Delta\dot{i}_q=\frac{1}{L_S}\Delta v_{sq}-\omega_{PLL0}\Delta i_d \tag{37}$$

$$\Delta\dot{v}_{sd}=k_{ii}\Delta i_{dref}+(\omega_{PLL0}^2L_S-k_{ii})\Delta i_d-\omega_{PLL0}\Delta v_{sq} \tag{38}$$

$$\Delta\dot{v}_{sq}=k_{ii}\Delta i_{qref}+(\omega_{PLL0}^2L_S-k_{ii})\Delta i_q+\omega_{PLL0}\Delta v_{sd} \tag{39}$$

$$i_{dc0}\Delta v_{dc}-v_{sd0}\Delta i_d-i_{d0}\Delta v_{sd}-v_{sq0}\Delta i_q-i_{q0}\Delta v_{sq}=0 \tag{40}$$

#### 4.3.2 Solar PV Integrated Multi-machine Model

In Sect. 4.1, the linearized multi-machine model of synchronous machine had been developed. In this section, after modeling the individual components of PV system and linearizing the system equations, the development of the multi-machine model integrated with solar PV is done. Equations (7)–(19) of the multi-machine model and (34)–(40) of the solar PV model can be combined and written as:

$$\begin{aligned}\begin{bmatrix}\Delta\dot{x}\\ \Delta\dot{x}_{solar}\end{bmatrix}&=\begin{bmatrix}A_1&0\\0&A_{solar}\end{bmatrix}\begin{bmatrix}\Delta x\\ \Delta x_{solar}\end{bmatrix}+\begin{bmatrix}B_1\\0\end{bmatrix}\Delta I_g\\&\quad+\begin{bmatrix}B_2\\0\end{bmatrix}\Delta V_g+\begin{bmatrix}E_1&0\\0&E_{solar}\end{bmatrix}\begin{bmatrix}\Delta u\\ \Delta u_{solar}\end{bmatrix}\end{aligned} \tag{41}$$

$$0=\begin{bmatrix}C_1&0\end{bmatrix}\begin{bmatrix}\Delta x\\ \Delta x_{solar}\end{bmatrix}+D_1\Delta I_g+D_2\Delta V_g \tag{42}$$

$$0 = \begin{bmatrix} C_2 & 0 \end{bmatrix} \begin{bmatrix} \Delta x \\ \Delta x_{solar} \end{bmatrix} + D_3 \Delta I_g + D_4 \Delta V_g + D_5 \Delta V_l \quad (43)$$

$$0 = \begin{bmatrix} 0 & C_{3solar} \end{bmatrix} \begin{bmatrix} \Delta x \\ \Delta x_{solar} \end{bmatrix} + D_6 \Delta V_g + D_7 \Delta V_l \quad (44)$$

where

$$x = \begin{bmatrix} x_1^t & \ldots & x_m^t \end{bmatrix}^t$$

$$x_i = \begin{bmatrix} \delta_i & \omega_i & E'_{qi} & E'_{di} & E_{fdi} & V_{Ri} & R_{fi} \end{bmatrix}^t$$

$$x_{solar} = \begin{bmatrix} i_{mp} & v_{DC} & i_d & i_q & v_{sd} & v_{sq} \end{bmatrix}^t$$

$$I_g = \begin{bmatrix} I_{d1} & I_{q1} & \ldots & I_{dm} & I_{qm} \end{bmatrix}^t$$

$$V_g = \begin{bmatrix} \theta_1 & V_1 & \ldots & \theta_m & V_m \end{bmatrix}^t$$

$$V_l = \begin{bmatrix} \theta_{m+1} & V_{m+1} & \ldots & \theta_n & V_n \end{bmatrix}^t$$

$$u = \begin{bmatrix} u_1^t & \ldots & u_m^t \end{bmatrix}^t$$

$$u_i = \begin{bmatrix} T_{Mi} & V_{refi} \end{bmatrix}^t$$

$$u_{solar} = \begin{bmatrix} v_{mp} & i_{dref} & i_{qref} \end{bmatrix}^t$$

and

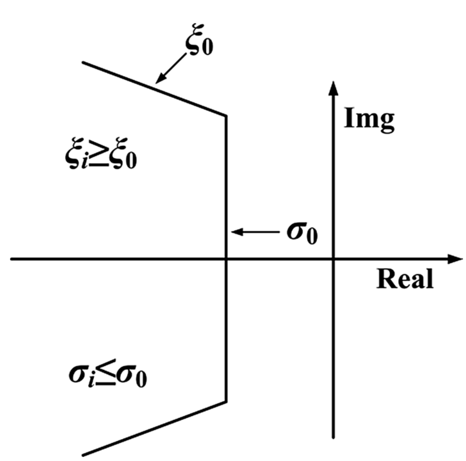


**Fig. 4** Domain of eigenvalue locations for objective function ($J$) [44]

$$A_{solar} = \begin{bmatrix} 0 & -\frac{D_0}{L} & 0 & 0 & 0 & 0 \\ \frac{D_0}{C} & 0 & 0 & 0 & 0 & 0 \\ 0 & 0 & 0 & \omega_{PLL0} & \frac{1}{L_S} & 0 \\ 0 & 0 & -\omega_{PLL0} & 0 & 0 & \frac{1}{L_S} \\ 0 & 0 & \omega_{PLL0}^2 L_S - k_{ii} & 0 & 0 & -\omega_{PLL0} \\ 0 & 0 & 0 & \omega_{PLL0}^2 L_S - k_{ii} & \omega_{PLL0} & 0 \end{bmatrix}$$

$$E_{solar} = \begin{bmatrix} \frac{1}{L} & 0 & 0 \\ 0 & 0 & 0 \\ 0 & 0 & 0 \\ 0 & 0 & 0 \\ 0 & k_{ii} & 0 \\ 0 & 0 & k_{ii} \end{bmatrix}$$

## 5 Objective Function

On being subjected to any disturbance, the rate of oscillation decay in the power system and its amplitude are governed respectively by the system's damping factor and damping ratio. Negative real parts of eigenvalues along with higher damping ratio signify a stable system [39]. Real and imaginary parts of eigenvalues provide the coefficient of damping. To tune the parameters of the controller using eigenvalue analysis, the objective function is evaluated in terms of two sub-objective functions (SOFs). First SOF is tasked with the minimization of real part of eigenvalues and second SOF targets maximization of the damping ratio, as depicted in Fig. 4 [44]. The objective function is mathematically represented as follows:

$$\text{Minimize, } J = J_1 + J_2 \quad (45)$$

where $J_1 = \sum_{k=1}^{m} (\sigma_0 - \sigma_k)^2$ and $J_2 = \sum_{k=1}^{m} (\xi_0 - \xi_k)^2$ where, the number of EMs is denoted by $m.J_1$ represents the first SOF related to the real part of eigenvalues and $J_2$ is the second SOF related to the damping ratio. $\sigma_0$ and $\xi_0$ are taken to be – 0.5 and 0.1 respectively [43]. The following constraints are to be satisfied by the objective function $J$:

$$\left.\begin{array}{l} K_{PSS}^{\min} \leq K_{PSS} \leq K_{PSS}^{\max} \\ T_1^{\min} \leq T_1 \leq T_1^{\max} \\ T_2^{\min} \leq T_2 \leq T_2^{\max} \\ T_3^{\min} \leq T_3 \leq T_3^{\max} \\ T_4^{\min} \leq T_4 \leq T_4^{\max} \end{array}\right\} \text{PSS parameters} \quad (46)$$

A two-staged PSS is considered for the study. Phase-lead time constants $T_1$ and $T_1$ and phase-lag time constants $T_1$ and

$T_1$ varies from 0.06 to 1.0 s and 0.01 to 0.05 s respectively. The gain $K_{PSS}$ is bounded by [0.01, 50]. $T_w$ is fixed to 10 s.

## 5.1 Optimization Techniques for Tuning PSS parameters

### 5.1.1 CDO Algorithm [50]

Collective decision optimization algorithm (CDO) as presented in [47] is based on the decision making capabilities of human beings dictating their social behavior. Whenever faced with a problem, human beings have a natural tendency to form a group having persons with diverse capabilities to arrive at a decision or a solution. Exchange and selection of ideas amongst all group members take place and the best idea amongst all is finally selected. The decision making abilities are classified into the following different phases [47]:

**5.1.1.1 Creation of Group** A group comprising of P members is randomly initialized within the search space having dimension D as follows:

$$K_i^j = LB^j + rand(0,\ 1) \times \left(UB^j - LB^j\right) \tag{47}$$

where $i = 1, 2, 3, \ldots\ldots, P$; $j = 1, 2, 3, \ldots\ldots D$. *rand* denotes any random number in the interval [0, 1], and *LB* and *UB* symbolizes the lower and upper limits of the independent variables.

**5.1.1.2 Experience Phase** During any meeting between the group members, agents lay their plans which are founded on their individual experiences. This is the present best position of the agent $\Phi_A$ which can be stated as:

$$K_{i\,new} = K_i + rand(0,\ 1) \times step\_size \times d_0 \tag{48}$$

$$d_0 = \Phi_A - K_i \tag{49}$$

where *rand* is any random number in the range [0, 1],*step_size* signifies the step size of current iteration, and *d* signifies the direction of selection of next agent.

**5.1.1.3 Others' Idea Phase** Interchange of ideas between the agents occurs in this phase and others' ideas get accepted by an agent only if they are superior to her/his idea. If any agent $K_j$, is selected randomly from the population to exchange idea with $K_i$, the one having better quality of idea is selected as follows:

$$K^{(1)}_{i\,new} = K_{i\,new} + rand(0,\ 1) \times step\_size \times d_1 \tag{50}$$

$$d_1 = beta_1 \times d_0 + beta_2 \times \left(X_j - X_i\right) \tag{51}$$

where *j* represents the agent selected from [1, P], $d_1$ represents a new direction for selection of next agent and $beta_1$ and $beta_2$ represents any two numbers randomly selected from the intervals [−1, 1] and [0, 2] respectively.

**5.1.1.4 Group-thinking Phase** In this phase, the manner in which agents' decisions gets motivated is dictated by the direction in which the maximum ideas are inclined. The present position of the group thinking is considered to be the geometric center ($\Phi_G$) of each agent which is expressed as:

$$\Phi_G = \frac{1}{P}\left(K_1, K_2, \ldots\ldots\ldots,\ K_P\right) \tag{52}$$

The agent's updated position is obtained as follows:

$$newK_i^{(2)} = newK_i^{(1)} + rand(0,1) \times step\_size \times d \tag{53}$$

$$d_2 = beta_1 \times d_1 + beta_2 \times \left(\Phi_G - K_i\right) \tag{54}$$

where $d_2$ is the new direction of progress of ideas.

**5.1.1.5 Leader Phase** The group leader is the ultimate decision maker and dictates the direction of movement of ideas as well as the final output. Mathematically this can be represented as follows:

$$newK_i^{(3)} = newK_i^{(2)} + rand(0,1) \times step\_size \times d_3 \tag{55}$$

$$d_3 = beta_1 \times d_2 + beta_2 \times \left(\Phi_L - K_i\right) \tag{56}$$

where $d_3$ is the new direction of progress of ideas. Leader ($\Phi_L$) represents the agent with the best idea in the group. Leader can change his/her idea by himself/herself. This algorithm uses random walk strategy for local search.

$$newK_p = \Phi_L + W_p \quad (p = 1, 2, 3, 4, 5) \tag{57}$$

where $W_p$ signifies any vector selected randomly from the interval [0, 1].

**5.1.1.6 Innovation Phase** In this phase, the decision making process is improved by perturbing the existing variables (mutation factors) and can be implemented as follows:

$$\begin{aligned} &rand1 \le M \\ &newK_i^{(4)} = newK_i^{(4)} \\ &newK_i^{(4,F)} = LB(F) + rand2 \times (UB(F) - LB(F)) \end{aligned} \tag{58}$$

where *M* is the mutation factor employed to evade premature convergence, *rand*1 and *rand*2 are random numbers within

[0, 1] and uniformly distributed, and $F$ is randomly generated within interval [1, D].

Selection of proper *step_size* is a deciding factor for exploration and exploitation capabilities of the algorithm. In the initial stages, if the larger, it will ensure better exploration whereas smaller values in the later parts of the algorithm ensure proper exploitation of the population. The *step_size* is calculated as follows:

$$step\_size\,(t) = 2 - 1.7\left(\frac{t-1}{T-1}\right) \tag{59}$$

where $t$ signifies the current iteration and $T$ signifies the maximum iteration count.

#### 5.1.2 Application of CDO Algorithm

The steps followed to apply CDO for parameter tuning of PSS are described below:

**Step 1:** Initialize randomly a group of P members (PSS gain and lead-lag time constant) in the search space D within their upper and lower bounds based on (46). Choose maximum fitness evaluation (maxFE).
**Step 2:** Perform SSSA of the system for each member in group and obtain eigenvalues. Check whether the inequality constraints of (46) are satisfied by the eigenvalues.
**Step 3:** Compute the fitness function (plan quality) as per (45) for each group and store total number of fitness evaluation in a variable FE.
**Step 4:** Detect the new best position of agents ($K_{inew}$) based on their fitness values (quality of plan) to form the modified group set.
**Step 5:** Update the members of group in all phases of CDO employing (47)-(59).
**Step 6:** Determine the best plan and best group. Best plan is identified as minimum of the fitness function evaluated for each solution set and best group is the solution set corresponding to the best plan.
**Step 7:** Go to step 5 and repeat until value of FE reaches maxFE.

#### 5.1.3 Grasshopper Optimization Algorithm (GOA)

In Grasshopper Optimization Algorithm, the swarming behaviour exists both in nymph and adult stage. In the larval stage, movement of the swarm is slow, whereas, in the adult stage, the swarm can move long distances and exhibit abrupt motion. The grasshopper algorithm as described in [48] updates its swarm using the following set of equations:

$$P_i = S_i + G_i + W_i \tag{60}$$

where $P_i$ denotes the position of the $i$th grasshopper (*GH*), $S_i$ denotes the social interaction of the *GHs*,$G_i$ represents the gravity force acting on the $i$th *GH* and $W_i$ represents the wind advection.

$$S_i = \sum_{\substack{k=1 \\ k\neq i}}^{N} s\,(d_{ik})\,\hat{d}_{ik} \tag{61}$$

where $N$ denotes the number of *GHs*, $d_{ik}$ denotes distance from $i$ to $k$th and calculation of *GH*s is done as follows: $d_{ik} = |P_k - P_i|$ and $\hat{d}_{ik} = \frac{P_k - P_i}{d_{ik}}$ represents a unit vector from $i$th *GH* to $k$th *GH*.$s$ denotes the social forces and is considered as:

$$s(r) = fe^{\frac{-r}{l}} - e^{-r} \tag{62}$$

where $f$ denotes the attraction intensity between the *GHs* and $l$ denotes the attraction length scale. Gravitational force $G$ is designed as:

$$G_i = -g\hat{c}_g \tag{63}$$

where $g$ denotes gravitational constant and $\hat{c}_g$ is a unit vector to the earth's center. Wind advent component is calculated as:

$$W_i = u\hat{b}_w \tag{64}$$

where $u$ is drift constant and $\hat{b}_w$ is a unit vector in the wind's direction.

Substituting values of the parameters $S, G, W$ in (60), the position of the *GH* can be expanded as:

$$P_i = \sum_{\substack{k=1 \\ k\neq i}}^{N} s(|P_k - P_i|)\frac{P_k - P_i}{d_{ik}} - g\hat{c}_g + u\hat{b}_w \tag{65}$$

But (65) cannot be directly used for solving optimization problems as the *GHs* are quick to reach comfort zone thereby causing the swarm to diverge. Following equation shows the modified version of (65) for solving optimization problems:

$$P_i^d = c\left(\sum_{\substack{k=1 \\ k\neq i}}^{N} c\frac{ub^d - lb^d}{2}s(r)\left(\left|P_k^d - P_i^d\right|\right)\frac{P_k - P_i}{d_{ik}}\right) + \hat{T}^d \tag{66}$$

where $ub^d$ and $lb^d$ represent respectively the upper bound and lower bound in the $d$th dimension, $T^d$ represents the value of target in $d$th dimension, $c$ is the shrinking coefficient to decrease the comfort, attraction and repulsion zones of the *GHs*. The coefficient $c$ is calculated as:

$$c = \max(c) - Iter\left(\frac{\max(c) - \min(c)}{\max Iter}\right) \tag{67}$$

where max($c$) and min($c$) represent the maximum and minimum values of $c$.*Iter* and max *Iter* represent the current iteration and maximum iterations respectively.

#### 5.1.4 Application of GOA Algorithm

The steps relating the application of GOA to the stability problem are as follows:

**Step 1:** Specify the swarm size and initialize the swarm (SW) randomly for the same. Set the number of control parameters (GHs) of SW within lower and upper limits. Select maximum number of fitness evaluation (maxFE).
**Step 2:** Inspect small signal stability for each GH of SW and obtain the eigenvalues that lies within limits of the control variables.
**Step 3:** Evaluate eigenvalue based fitness function using each swarm set, and store total fitness evaluations (FE).
**Step 4:** Select the best swarm set (GHbest) based on their fitness values and form the updated swarm set.
**Step 5:** Update swarm using (65).
**Step 6:** Determine the best fitness (minimum fitness function value) and also the best swarm set.
**Step 7:** Return to step 5 and repeat till the FE equals the pre-defined maxFE.

#### 5.1.5 Salp Swarm Algorithm (SSA)

Salp Swarm Algorithm (SSA) as reported in [49] is a recently developed meta-heuristic that exploits the food searching technique of salps. Salp swarms form a chain to move in search of food. The swarm is modeled after leaders (*LD*) and followers (*FL*) are identified. The salp at the beginning of the chain becomes *LD* and is tasked with guiding the whole swarm. All other members are *FL*. Position update of *LD* in SSA takes place as per the following set of equations:

$$x_j^1 = \begin{cases} F_j + c_1\left((ub_j - lb_j)c_2 + lb_j\right) & c_3 \geq 0 \\ F_j - c_1\left((ub_j - lb_j)c_2 + lb_j\right) & c_3 < 0 \end{cases} \tag{68}$$

where $x_j^1$ denotes the position of the *LD* in *j*th dimension, $F_j$ is the location of food, *ub* and *lb* denotes the upper and lower limits and $c_1$, $c_2$ and $c_3$ are random numbers. $c_1$ decides the exploration and exploitation capability of SSA and can be defined as:

$$c_1 = 2e^{\left(-\frac{4l}{L}\right)^2} \tag{69}$$

where $l$ and $L$ signifies the present and maximum number of iterations.

$c_2$ and $c_3$ forecasts the new position of *FLs* as well as the step size. Updated positions of the *FLs* are obtained as:

$$x_j^i = \frac{1}{2}at^2 + v_0 t \tag{70}$$

where $i \geq 2$, $x_j^i$ signifies position of *i*th *FL* in *j*th dimension, $t$ signifies time, $v_0$ signifies initial speed of motion, and $a = \frac{v_{final}}{v_0}$, where $v = \frac{(x - x_0)}{t}$.

Considering initial speed $v_0 = 0$, the above equation can be modified as:

$$x_j^i = \frac{1}{2}\left(x_j^i + x_j^{i-1}\right) \tag{71}$$

where $i \geq 2$ and $x_j^i$ represents position of *i*th *FL* in *j*th dimension.

The salp chain is simulated using (68) and (71).

### 5.2 Application of SSA Algorithm

The steps of the SSA applied to the stability problem are described as follows:

**Step 1:** Randomly initialize the swarm (SW) comprising of the salps (control parameters such as PSS gain and lead-lag time constants) within their upper and lower bounds for a particular swarm size. Specify the maximum number of fitness evaluation (maxFE).
**Step 2:** Perform SSSA for each salp chain of SW and obtain the eigenvalues.
**Step 3:** Evaluate fitness function (eigenvalue- based) for each swarm set, and store total fitness evaluations in FE.
**Step 4:** Identify best swarm set (SWbest) based on the fitness.
**Step 5:** Update the swarm using (68) and (71).

**Table 1** Loading conditions for Case 1.1

| | P (p.u) | Q (p.u) |
|---|---|---|
| Generator | | |
| G1 | 0.9649 | 0.2330 |
| G2 | 1.0000 | −0.1933 |
| G3 | 0.4500 | −0.2668 |
| Load | | |
| L5 | 0.7000 | 0.3500 |
| L6 | 0.5000 | 0.3000 |
| L8 | 0.6000 | 0.2000 |
| Local load at G1 | 0.6000 | 0.2000 |

**Table 2** Tuned PSS parameters obtained using various algorithms

| | CDO | GOA | SSA |
|---|---|---|---|
| Generator1 | | | |
| *Kpss* | 2.569100 | 18.96000 | 28.54000 |
| $T_1$ (s) | 1.252700 | 1.500000 | 0.603000 |
| $T_2$ (s) | 0.071439 | 0.150000 | 0.026000 |
| $T_3$ (s) | 1.291200 | 1.136600 | 0.809000 |
| $T_4$ (s) | 0.117900 | 0.014153 | 0.048400 |
| Generator2 | | | |
| *Kpss* | 1.917600 | 3.564700 | 2.734000 |
| $T_1$ (s) | 0.569380 | 1.457100 | 1.436000 |
| $T_2$ (s) | 0.027684 | 0.010000 | 0.013000 |
| $T_3$ (s) | 1.147500 | 0.217620 | 0.902000 |
| $T_4$ (s) | 0.025351 | 0.010082 | 0.010000 |
| Generator3 | | | |
| *Kpss* | 6.316000 | 4.846500 | 4.085000 |
| $T_1$ (s) | 0.188030 | 0.745690 | 0.100000 |
| $T_2$ (s) | 0.131070 | 0.020197 | 0.020200 |
| $T_3$ (s) | 0.206240 | 0.317110 | 0.247000 |
| $T_4$ (s) | 0.150000 | 0.010000 | 0.150000 |

**Step 6:** Obtain best fitness value as the minimum fitness function value and the SWbest.
**Step 7:** Repeat from step 5 till the predefined maxFE.

## 6 Simulations and Results

This section presents analysis of system performances after applying the SSA algorithm. Eigenvalues determined by SSA are used to assess the system stability and compared to those obtained using GOA and CDO. Results establish superiority of SSA over other mentioned optimization techniques in evaluating the small signal stability of the system. WSCC three machine, nine bus system [1] have been considered to carry out eigenvalue analysis when subjected to different operating conditions and are coded in MATLAB platform. The system data of WSCC 3-Machine 9-Bus system is given in [1]. All the calculations are made with system frequency of 60 Hz and base MVA as 100.

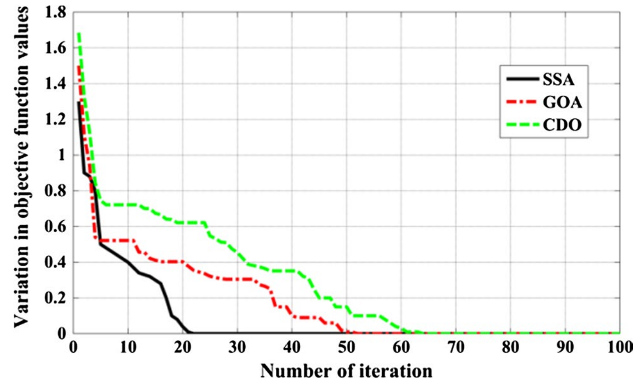


**Fig. 5** Convergence characteristics obtained by different algorithms

### 6.1 Case 1: Results Related to PSS Parameter Tuning

The most important task is the proper tuning of PSS parameters. Properly tuned parameters help to increase system stability but, badly tuned parameters may lead the system to instability. The power system is nonlinear and its varying operating condition makes tuning as a complex task. Tuning is done based on the characteristics of the generator system. To demonstrate efficiency of the proposed algorithm, different cases have been considered as discussed below:

#### 6.1.1 Case 1.1

To illustrate the effectiveness of the proposed algorithm, PSS were installed in all the machines for mitigating low frequency oscillations. Electromechanical modes and their damping ratios for the different algorithms used are presented in Table 2.

Tuning of PSS parameters have been done for *Case 1.1* using loading conditions presented in Table 1. The tuned PSS parameters obtained after applying the optimization algorithms are presented in Table 2. It can be observed from Table 3 that SSA obtained the best tuning parameter settings for *Case 1.1*.

Fifty trial runs of the algorithms have been carried out for 100 iterations each. The convergence characteristics of the best parameter set obtained for each of the algorithms are

**Table 3** EMs and their corresponding damping ratios obtained for *Case 1.1*

| No stabilizer | CDO based PSS | GOA based PSS | SSA based PSS | Dominant machine variables |
|---|---|---|---|---|
| $-1.436 \pm j13.275$, $\xi = 0.10755$ | $-2.3783 \pm j13.389$, $\xi = 0.17489$ | $-5.9328 \pm j13.76$, $\xi = 0.39581$ | $\mathbf{-6.324 \pm j13.453}$, $\mathbf{\xi = 0.4254}$ | $\delta_3, \omega_3$ |
| $-0.37734 \pm j9.131$, $\xi = 0.04129$ | $-1.7768 \pm j9.8859$, $\xi = 0.17690$ | $-2.2506 \pm j9.0169$, $\xi = 0.24217$ | $\mathbf{-2.568 \pm j8.984}$, $\mathbf{\xi = 0.2748}$ | $\delta_2, \omega_2$ |

**Table 4** EMs and their corresponding damping ratios obtained for *Case 1.2*

| No stabilizer | CDO based PSS | GOA based PSS | SSA based PSS | Dominant machine variables |
|---|---|---|---|---|
| $-0.907 \pm j13.57$, $\xi = 0.066656$ | $-1.8462 \pm j13.592$, $\xi = 0.13459$ | $-6.4239 \pm j13.604$, $\xi = 0.42699$ | $\mathbf{-6.567 \pm j13.1568}$, $\mathbf{\xi = 0.4466}$ | $\delta_3, \omega_3$ |
| $-0.185 \pm j9.0462$, $\xi = 0.020433$ | $-1.9521 \pm j9.7341$, $\xi = 0.19663$ | $-3.8959 \pm j9.0331$, $\xi = 0.39603$ | $\mathbf{-3.8671 \pm j8.5976}$, $\mathbf{\xi = 0.4102}$ | $\delta_2, \omega_2$ |

compared in Fig. 5. It can be observed that SSA obtained fastest convergence as compared to GOA and CDO.

**Table 5** Loading conditions for *Case 1.2*

| | P (p.u) | Q (p.u) |
|---|---|---|
| Generator | | |
| G1 | 1.7164 | 0.6205 |
| G2 | 1.6300 | 0.0665 |
| G3 | 0.8500 | −0.1086 |
| Load | | |
| L5 | 1.2500 | 0.5000 |
| L6 | 0.9000 | 0.3000 |
| L8 | 1.0000 | 0.3500 |
| Local load at G1 | 1.0000 | 0.3500 |

The final value of the objective function is $J=0$ for all the algorithms which signifies that all modes have been shifted to the specified D-space in the S-plane of Fig. 5.

### 6.1.2 Case 1.2

To establish the robustness of the proposed algorithm, the EMs are obtained for another loading condition using the same tuning parameters obtained for *Case 1.1* listed in Table 3. The EMs and damping ratios for this case are listed in Table 4 demonstrating the superiority of SSA over CDO and GOA. Table 5 presents the loading conditions for this case.

### 6.1.3 Case 1.3

Similar pattern in the performances of the algorithms can be observed from Table 6 for same tuning parameters of *Case 1.1* when the loading condition is changed again.

Table 7 preents the loading conditions for this case.

**Table 7** Loading conditions for *Case 1.3*

| | Heavily loaded | |
|---|---|---|
| | P (p.u) | Q (p.u) |
| Generator | | |
| G1 | 3.5730 | 1.8143 |
| G2 | 2.2000 | 0.7127 |
| G3 | 1.3500 | 0.4313 |
| Load | | |
| L5 | 2.0000 | 0.9000 |
| L6 | 1.8000 | 0.6000 |
| L8 | 1.6000 | 0.6500 |
| Local load at G1 | 1.6000 | 0.6500 |

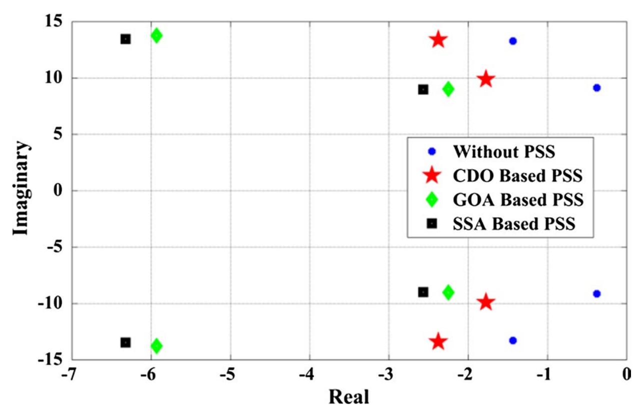


**Fig. 6** EMs obtained for *Case 1.1*

It is quite obvious from the Tables 2, 4 and 6 that SSA is capable in shifting EMs (real parts) to the left half of S plane as well as enhances the damping ratios in comparison to GOA and CDO. PSS parameters are tuned in *Case* 1.1 for a particular operating condition. In order to establish

**Table 6** EMs and their corresponding damping ratios obtained for *Case 1.3*

| No stabilizer | CDO based PSS | GOA based PSS | SSA based PSS | Dominant machine variables |
|---|---|---|---|---|
| $-0.79932 \pm j13.633$, $\xi = 0.058531$ | $-1.5661 \pm j13.578$, $\xi = 0.11458$ | $-6.438 \pm j13.463$, $\xi = 0.43141$ | $\mathbf{-6.657 \pm j12.983}$, $\mathbf{\xi = 0.4563}$ | $\delta_3, \omega_3$ |
| $-0.16828 \pm j8.7924$, $\xi = 0.019136$ | $-2.0795 \pm j\,9.5543$, $\xi = 0.21267$ | $-3.8251 \pm j7.8673$, $\xi = 0.43726$ | $\mathbf{-3.937 \pm j7.3902}$, $\mathbf{\xi = 0.4702}$ | $\delta_2, \omega_2$ |

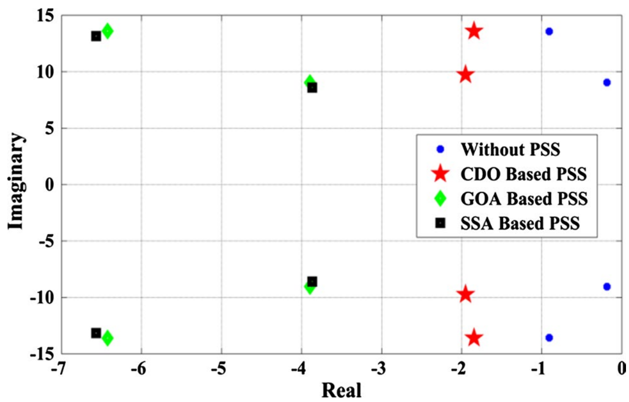


**Fig. 7** EMs obtained for *Case 1.2*

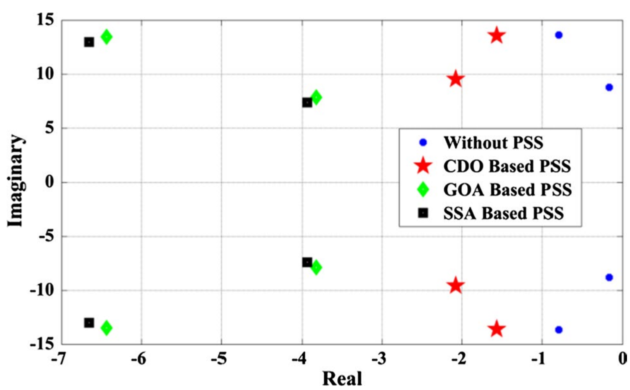


**Fig. 8** EMs obtained for Case 1.3

robustness of the proposed algorithm, SSSA studies are carried out for different operating conditions using the tuned parameters of PSS obtained from *Case 1.1*. SSA based PSS shows superior performance and attains enhanced damping as compared to GOA and CDO based PSS for each operating condition.

Figures 6, 7, and 8, represent system eigenvalues obtained for *Case 1.1*, *Case 1.2* and *Case 1.3* respectively. It is observed that the system eigenvalues are shifting further towards the left half of s-plane and also the damping ratios are being improved in each case for SSA as compared to those of GOA and CDO. This indicates the efficiency of SSA technique in tuning PSS parameters and stabilizing the system under various operating conditions.

## 6.2 Case 2: System's Time Domain Response for Case 1

To illustrate superiority of the proposed algorithm, a three-phase fault is applied near bus 5 at time 0.1 s, which is cleared at 0.2 s without tripping any line. Study of the change in speed deviation is enough for arriving at a conclusion regarding system stability. Therefore, only the change in rotor speed deviations obtained after time domain simulation is demonstrated in Figs. 9, 10 and 11. for best values obtained by each algorithm. These figures show the response of $\Delta\omega_{12}$ and $\Delta\omega_{13}$ obtained by each of the algorithms, when the system is subjected to *Case 1.1*, *Case 1.2* and *Case 1.3*. It is observed that the newly proposed SSA keeps the system more stabilized as compared to other optimization techniques and also requires lesser settling time to mitigate the system oscillations as compared to GOA and CDO.

## 6.3 Case 3: Solar PV is connected to the System

All the calculations are made with system frequency of 60 Hz and base MVA as 100. For the purpose of simulating multi-machine power system model with integrated solar PV at transmission level, in bus number 5, 6 and 8 of the test system (WSCC 3-Machine 9-Bus), a 50 MW, 11 kV solar PV has been connected. Results obtained after using the iterative process for calculating the series and

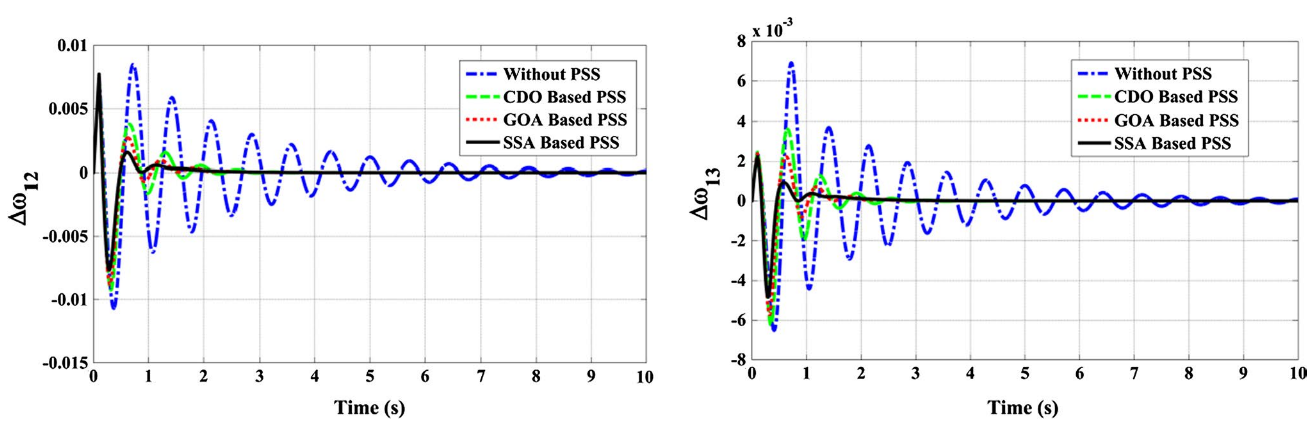


**Fig. 9** Change in $\Delta\omega_{12}$ and $\Delta\omega_{13}$ for *Case 1.1*

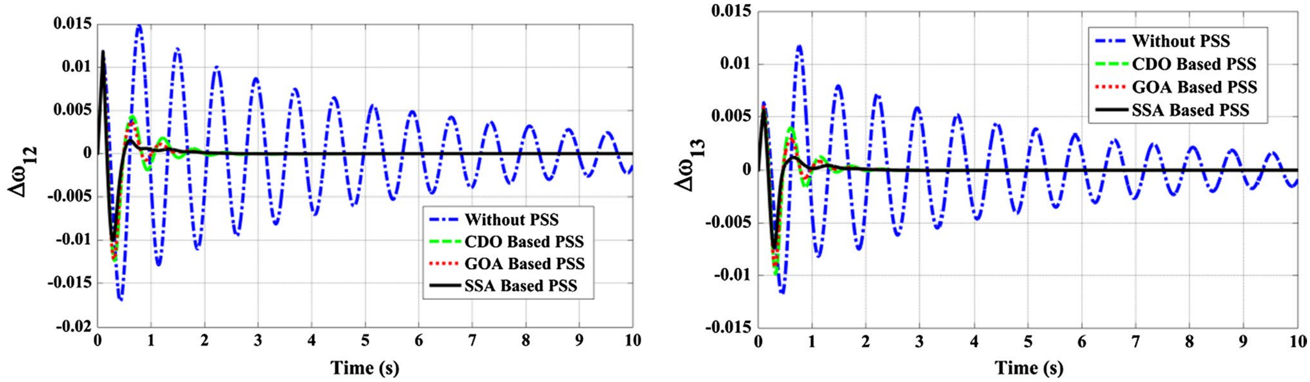


**Fig. 10** Change in $\Delta\omega_{12}$ and $\Delta\omega_{13}$ for *Case 1.2*

**Table 8** Solar Module parameters of Kyocera 200 GT model at STC

| Parameters | Value Obtained when PV installed at bus 5 |
|---|---|
| $I_{PVn}$(in $A$) | 8.21451 |
| $I_{PV}$(in $A$) | 8.21451 |
| $R_S$(in Ω) | 0.22000 |
| $R_P$(in Ω) | 412.998 |
| $I_0$(in $A$) | 9.82500e–8 |
| $I_{0n}$(in $A$) | 9.852500e–8 |

**Table 9** Maximum power, current and voltage of module at 600 $W/m^2$ and T = 323 K

| G (in $W/m^2$) | T (in K) | $I_{mp}$(in A) | $V_{mp}$(in V) | $P_{mp}$(in W) |
|---|---|---|---|---|
| 600 | 323 | 4.4952 | 23.318 | 104.82 |

**Table 10** Parameters of boost converter

| Duty cycle ($D$) | Ripple current ($\Delta I_L$) | Inductance ($L$) | Ripple voltage ($\Delta V_{OUT}$) | DC link capacitance ($C$) |
|---|---|---|---|---|
| 0.34972 | 318.49 | 0.00099474 | 17.517 | 0.004138 |

parallel parasitic resistance ($R_S$ and $R_P$) on *Kyocera 200 GT* solar module [45] is shown in Table 8. These results have been obtained at Standard Temperature Condition (STC) i.e. at solar irradiation of 1000 W/m$^2$ with AM 1.5 at 25 °C.

These results have been compared with those given in [13] and they are found to be almost similar. An initial operating condition of the entire system is assumed at solar irradiation, $G = 600$ W/m$^2$ and temperature, $T = 50$ °C. All the calculations made henceforth are with respect to this initial operating condition. Using the algorithm given in [46], the maximum current and voltage output from the solar module is obtained at $G = 600\ W/m^2$ and $T = 50$ °C. The result is given below in Table 9.

Next, it was essential to calculate the number of modules that has to be connected in series–parallel combination in order to meet the 50 MW, 11 kV requirement. Required current output from the PV array is calculated as $\frac{50\,MW}{11\,kV} \approx 4545.4545A$.

Now, for 4545.4545 $A$ dc current from the solar array, number of modules needed to be connected in parallel is calculated as $n_p = \frac{4545.4545}{4.4952} \approx 1011$. Also the number of modules to be connected in series for 11 kV requirement is calculated as $n_S = \frac{11\,kV}{23.318} \approx 472$.

Next, the duty cycle ($D$), Inductance ($L$) and DC-Link Capacitance ($C$) of the Boost Converter is to be calculated are shown is Table 10.

Here, solar PV is connected at load bus (5 or 6 or 8) shown in Fig. 11. The initial conditions for solar generators are given in Tables 8, 9 and 10. The active power supplied by the solar PV to the WSCC 3 machine 9 bus system [1] (considering original system data) for each bus is 0.5 p.u, as shown in Fig. 11. Solar integrated system matrix was formed using (7)–(19) and (34)–(40).

The computed eigenvalues after the inclusion of solar PV are compared in Table 11. The table contains the electro-mechanical modes (mode #1 and mode #2) when solar PV is connected to bus 5 or 6 or 8 as shown in Fig. 12. The best location of solar PV is found at bus 5 since damping ratio improvement is highest when it is connected to this bus.

## 6.4 Case 4: PSSs are added to Case 3

The function of the PSS is to provide adequate damping torque to the rotor oscillations for mitigating LFOs. For getting effective results PSS needs to be allocated properly. The main objective of installing PSS is to improve the EMs in case 4, using the same tuning parameters obtained for *Case*

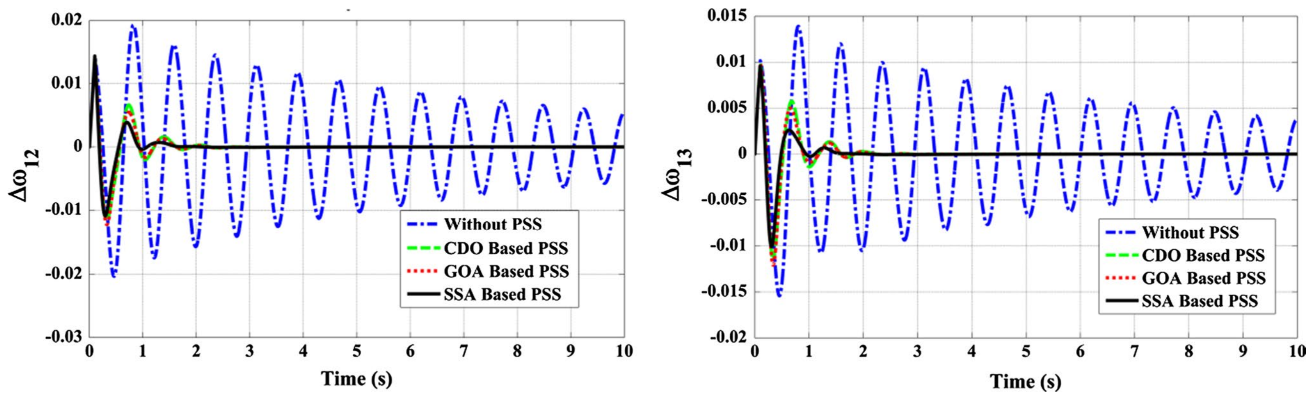


**Fig. 11** Change in $\Delta\omega_{12}$ and $\Delta\omega_{13}$ for *Case 1.3*

**Table 11** Eigenvalues and damping ratios (ξ) for different location of solar PV in WSCC system

| Mode number | Eigenvalues when solar PV is connected at bus 5 | Eigenvalues when solar PV is connected at bus 6 | Eigenvalues when solar PV is connected at bus 8 | Dominant states |
|---|---|---|---|---|
| #1 | $\mathbf{-0.8517 \pm j12.704}$ $\mathbf{\xi = 0.0669}$ | $-0.8481 \pm j12.7071$ $\xi = 0.0666$ | $-0.8547 \pm j12.704$ $\xi = 0.06710$ | $\delta_3, \omega_3$ |
| #2 | $\mathbf{-0.3268 \pm j8.3123}$ $\mathbf{\xi = 0.0393}$ | $-0.3186 \pm j8.3373$ $\xi = 0.0382$ | $-0.3131 \pm j8.3117$ $\xi = 0.0376$ | $\delta_2, \omega_2$ |
| #3 | $-5.545 \pm j7.9430$ $\xi = 0.572$ | $-5.5217 \pm j7.9449$ $\xi = 0.5707$ | $-5.5440 \pm j7.9456$ $\xi = 0.5722$ | $V_{R2}, E_{fd2}$ |
| #4 | $-5.2289 \pm j7.7903$ $\xi = 0.5573$ | $-5.2289 \pm j7.7968$ $\xi = 0.5570$ | $-5.2294 \pm j7.7873$ $\xi = 0.5575$ | $V_{R1}, E_{fd1}$ |
| #5 | $-5.3355 \pm j7.9228$ $\xi = 0.5586$ | $-5.3339 \pm j7.9219$ $\xi = 0.5585$ | $-5.3357 \pm j7.9240$ $\xi = 0.5585$ | $V_{R3}, E_{fd3}$ |
| #6 | $-5.0565$ $\xi = 1.000$ | $-5.0850$ $\xi = 1.000$ | $-5.0515$ $\xi = 1.000$ | $E'_{d2}$ |
| #7 | $-3.2258$ $\xi = 1.000$ | $-3.2258$ $\xi = 1.000$ | $-3.2258$ $\xi = 1.000$ | $E'_{d1}$ |
| #8 | $-3.2895$ $\xi = 1.000$ | $-3.3337$ $\xi = 1.000$ | $-3.2486$ $\xi = 1.000$ | $E'_{d3}$ |
| #9 | $-0.4437 \pm j1.3113$ $\xi = 0.3205$ | $-0.4455 \pm j1.2764$ $\xi = 0.3295$ | $-0.4406 \pm j1.3276$ $\xi = 0.5153$ | $E'_{q1}, R_{F1}$ |
| #10 | $-0.4511 \pm j0.7490$ $\xi = 0.5159$ | $-0.4471 \pm j0.7467$ $\xi = 0.5137$ | $-0.4510 \pm j0.7500$ $\xi = 0.5153$ | $E'_{q1}, R_{F1}$ |
| #11 | $-0.4461 \pm j0.5138$ $\xi = 0.65556$ | $-0.4414 \pm j0.5100$ $\xi = 0.6545$ | $-0.4469 \pm j0.5147$ $\xi = 0.6556$ | $E'_{q3}, R_{F3}$ |
| #12 | $-0.2189 \pm j1.0164$ $\xi = 0.2105$ | $-0.2328 \pm j1.0547$ $\xi = 0.2155$ | $-0.2831 \pm j0.9971$ $\xi = 0.2731$ | $\delta_1, \omega_1$ |
| #13 | $\pm j1.8757$ $\xi = 0.000$ | $\pm j1.8757$ $\xi = 0.000$ | $\pm j1.8757$ $\xi = 0.000$ | $i_q, v_{sq}$ |
| #14 | $\pm j1.8757$ $\xi = 0.000$ | $\pm j1.8757$ $\xi = 0.000$ | $\pm j1.8757$ $\xi = 0.000$ | $i_d, v_{sd}$ |
| #15 | $\pm j1.1327$ $\xi = 0.000$ | $\pm j1.1327$ $\xi = 0.000$ | $\pm j1.1327$ $\xi = 0.000$ | $i_{mp}, v_{DC}$ |

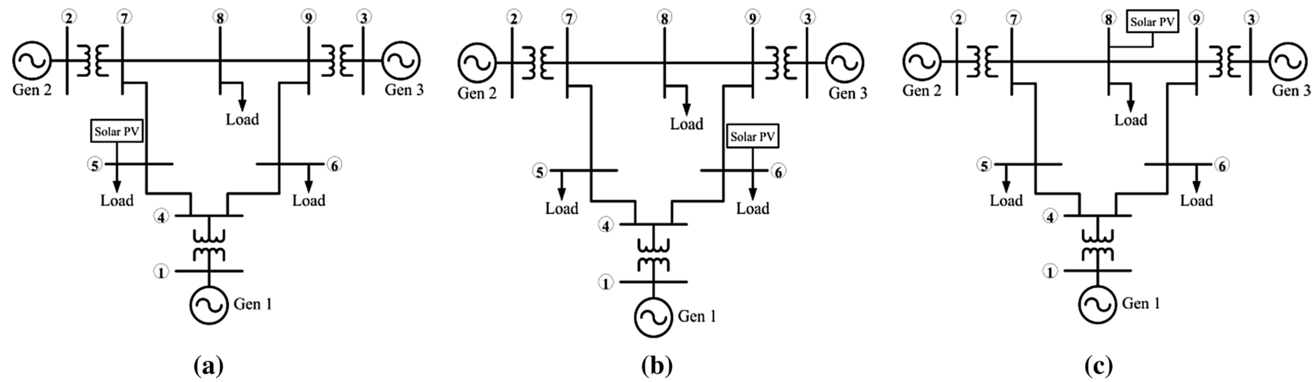


**Fig. 12** WSCC 3 machine 9 bus system equipped with solar PV at different location

**Table 12** EMs for the combination of solar PV, and PSS

| CDO based PSS and solar PV | GOA based PSS and solar PV | SSA based PSS and solar PV | Dominant state |
|---|---|---|---|
| $-2.549 \pm j6.893$, $\xi = 0.34684$ | $-2.935 \pm j6.534$, $\xi = 0.40975$ | $\mathbf{-3.6793 \pm j5.8309}$, $\mathbf{\xi = 0.41162}$ | $\delta_3, \omega_3$ |
| $-2.568 \pm j7.103$, $\xi = 0.09627$ | $-2.645 \pm j6.897$, $\xi = 0.3580$ | $\mathbf{-2.9215 \pm j6.4685}$, $\mathbf{\xi = 0.53364}$ | $\delta_2, \omega_2$ |

**Table 13** Comparison of the effects of coordinated controllers on small signal stability in presence of solar PV (Only the EMs) and without controllers

| WSCC system without controllers | SSA based WSCC together with PSS | SSA based WSCC together with PSS, and solar PV | Dominant state |
|---|---|---|---|
| $-0.8517 \pm j12.704$, $\xi = 0.0669$ | $-6.324 \pm j13.453$, $\xi = 0.4254$ | $\mathbf{-3.6793 \pm j5.8309}$, $\mathbf{\xi = 0.41162}$ | $\delta_3, \omega_3$ |
| $-0.3268 \pm j8.3123$, $\xi = 0.0393$ | $-2.568 \pm j8.984$, $\xi = 0.2748$ | $\mathbf{-2.9215 \pm j6.4685}$, $\mathbf{\xi = 0.53364}$ | $\delta_2, \omega_2$ |

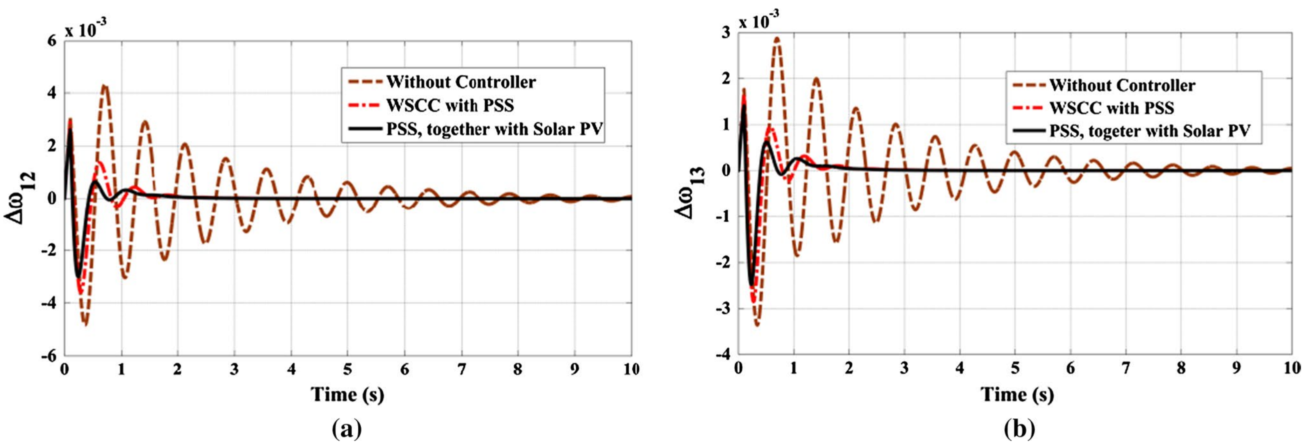


**Fig. 13** **a** Change in $\Delta\omega_{12}$ when fault occurs near bus 5; **b** change in $\Delta\omega_{13}$ when fault occurs near bus 5 (when solar PV is connected to the system)

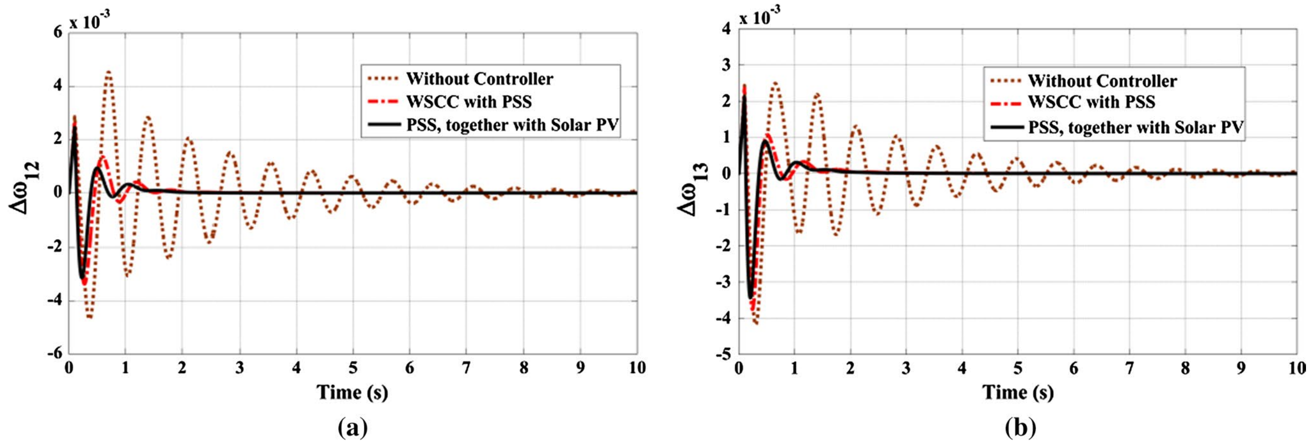


**Fig. 14** **a** Change in $\Delta\omega_{12}$ when fault occurs near bus 6; **b** Change in $\Delta\omega_{13}$ when fault occurs near bus 6 (when solar PV is connected to the system)

*1.1* listed in Table 3. Table 12 represents EMs for the combination of solar PV, and PSS.

Table 13 concludes the impact of coordinated controllers on small signal stability analysis when solar PV is included in it. It can be seen that when PV is connected to the system in presence of PSS gives better performance from overall system stability point of view.

### 6.5 Case 5: Time Domain Response for Case 4

Time domain simulations have been performed to demonstrate the efficiency of the system equipped with PSS and solar PV over the system having only PSS in improving overall system stability. Two different fault conditions are assumed:

Frequency plays a vital role in power system stability. All the generators in the system are synchronised at one frequency. If the frequency deviates from the nominal value, generators start to go out of synchronism. This triggers undesired events in the power system resulting in voltage, frequency, power imbalance which might even cause the system to collapse. Furthermore, continuous frequency deviations in the system cause oscillations of the rotor about its final equilibrium position, thereby introducing hunting. The hunting process occurs in a synchronous motor as well as in synchronous generators if an abrupt change in load occurs. To avoid these issues frequency deviations were investigated for the system equipped with DGs (solar PV), and PSS. Figures 13 and 14 represents frequency deviations for WSCC 3 machine 9 bus system equipped with PSSs and together with PSS and solar PV.

To observe the frequency deviations in these systems, fault is considered near the consumers end at bus 5 and bus 6. It is observed from the Figs. 13 and 14 that the peak overshoot as well as the settling time is lowest in case of solar PV together with PSS connected system as compared to the system equipped with only PSS connected system.

## 7 Conclusion

This work addressed renewable (solar) integration to the system studied in diverse operating conditions. System dynamics are largely affected with the integration of renewables in an integrated power network. An exhaustive small signal stability study on WSCC 3-machine 9-bus test system is presented under the following scenarios:

- ***System without renewable energy penetration and PSS***
- ***Addition of PSS***
- ***Renewables in presence of PSS***

Analysis of the results demonstrate better efficiency of renewable integrated power system together with PSS over PSS integrated power system in improving overall stability of the system.

This also paper presented a comparison between the performances of CDO, GOA and SSA in tuning the PSS parameters. Results show that best tuned parameter set for the PSS are obtained using SSA. It is also observed that damping ratios of the weakly damped oscillatory modes have improved after the addition of SSA based PSS, thereby enhancing the dynamic performance of system stability greatly. Time domain simulation results for different loading conditions show fastest settling of oscillations in case of SSA followed by GOA and CDO. All results establish SSA's superiority over GOA and CDO optimization techniques.

## References


1. Sauer PW, Pai MA (1998) Power system dynamics and stability, vol 101. Prentice hall, Upper Saddle River
2. Kundur P, Balu NJ, Lauby MG (1994) Power system stability and control, vol 7. McGraw-hill, New York
3. Padiyar KR (2008) Power system dynamics. BS publications, Hyderabad
4. Anderson PM, Fouad AA (2008) Power system control and stability. Wiley, Hoboken
5. Werner H, Korba P, Yang TC (2003) Robust tuning of power system stabilizers using LMI-techniques. IEEE Trans Control Syst Technol 11(1):147–152
6. Taranto GN, Chow JH (1995) A robust frequency domain optimization technique for tuning series compensation damping controllers. IEEE Trans Power Syst 10(3):1219–1225
7. Abido MA (2000) Pole placement technique for PSS and TCSC-based stabilizer design using simulated annealing. Int J Electr Power Energy Syst 22(8):543–554
8. Mondal D, Chakrabarti A, Sengupta A (2011) PSO based location and parameter setting of advance SVC controller with comparison to GA in mitigating small signal oscillations. In: 2011 International Conference on Energy, Automation and Signal, pp. 1–6, IEEE
9. Panda S, Padhy NP (2007) Regular paper robust coordinated design of PSS and TCSC using PSO technique for power system stability enhancement. J Electr Syst 3(2):109–123
10. Dong ZY, Makarov YV, Hill DJ (1997) Genetic algorithms in power system small signal stability analysis, pp 1–6
11. Zhang P, Coonick AH (2000) Coordinated synthesis of PSS parameters in multi-machine power systems using the method of inequalities applied to genetic algorithms. IEEE Trans Power Syst 15(2):811–816
12. Stativă A, Gavrilaş M, Stahie V (2012) Optimal tuning and placement of power system stabilizer using particle swarm optimization algorithm. In: 2012 International Conference and Exposition on Electrical and Power Engineering, pp 242–247. IEEE.
13. Safari A (2013) A PSO procedure for a coordinated tuning of power system stabilizers for multiple operating conditions. J Appl Res Technol 11(5):665–673
14. Mostafa HE, El-Sharkawy MA, Emary AA, Yassin K (2012) Design and allocation of power system stabilizers using the particle swarm optimization technique for an interconnected power system. Int J Electr Power Energy Syst 34(1):57–65
15. Panda S (2011) Robust coordinated design of multiple and multi-type damping controller using differential evolution algorithm. Int J Electr Power Energy Syst 33(4):1018–1030
16. Panda S (2009) Differential evolutionary algorithm for TCSC-based controller design. Simul Model Pract Theory 17(10):1618–1634
17. Ameli A, Farrokhifard M, Ahmadifar A, Safari A, Shayanfar HA (2013) Optimal tuning of Power System Stabilizers in a multi-machine system using firefly algorithm. In: 2013 12th International Conference on Environment and Electrical Engineering, pp 461–466, IEEE.
18. Elazim SA, Ali ES (2016) Optimal power system stabilizers design via cuckoo search algorithm. Int J Electr Power Energy Syst 75:99–107
19. Abido MA, Abdel-Magid YL (2002) Optimal design of power system stabilizers using evolutionary programming. IEEE Trans Energy Convers 17(4):429–436
20. Abido MA (1999) A novel approach to conventional power system stabilizer design using tabu search. Int J Electr Power Energy Syst 21(6):443–454
21. Abido MA (2000) Robust design of multimachine power system stabilizers using simulated annealing. IEEE Trans Energy Convers 15(3):297–304
22. Sambariya DK, Prasad R (2014) Robust tuning of power system stabilizer for small signal stability enhancement using metaheuristic bat algorithm. Int J Electr Power Energy Syst 61:229–238
23. Mishra S, Tripathy M, Nanda J (2007) Multi-machine power system stabilizer design by rule based bacteria foraging. Electr Power Syst Res 77(12):1595–1607
24. Dong ZY, Makarov YV, Hill DJ (1997) Genetic algorithms in power system small signal stability analysis.
25. Ameli A, Farrokhifard M, Ahmadifar A, Safari A, Shayanfar HA (2013) Optimal tuning of power system stabilizers in a multi-machine system using firefly algorithm. In: Environment and Electrical Engineering (EEEIC), 2013 12th International Conference on, pp 461–466, IEEE.
26. Saidur R, Rahim NA, Islam MR, Solangi KH (2011) Environmental impact of wind energy. Renew Sustain Energy Rev 15(5):2423–2430
27. Shahsavari A, Akbari M (2018) Potential of solar energy in developing countries for reducing energy-related emissions. Renew Sustain Energy Rev 90:275–291
28. Bambace LAW, Ramos FM, Lima IBT, Rosa RR (2007) Mitigation and recovery of methane emissions from tropical hydroelectric dams. Energy 32(6):1038–1046
29. Liu S, Liu PX, Wang X (2015) Stochastic small-signal stability analysis of grid-connected photovoltaic systems. IEEE Trans Industr Electron 63(2):1027–1038
30. Dahal S, Mithulananthan N, Saha T (2010) Investigation of small signal stability of a renewable energy based electricity distribution system. In: IEEE PES General Meeting, pp 1–8, IEEE
31. Ogata K (1995) Discrete-time control systems, vol. 2. Prentice Hall, Englewood Cliffs, pp 446–480
32. Rogers G (2012) Power system oscillations. Springer Science & Business Media, Berlin
33. Martins N (1986) Efficient eigenvalue and frequency response methods applied to power system small-signal stability studies. IEEE Trans Power Syst 1(1):217–224
34. Klein M, Rogers GJ, Moorty S, Kundur P (1992) Analytical investigation of factors influencing power system stabilizers performance. IEEE Trans Energy Convers 7(3):382–390
35. Martins N, Lima LT (1990) Determination of suitable locations for power system stabilizers and static VAR compensators for damping electromechanical oscillations in large scale power systems. IEEE Trans Power Syst 5(4):1455–1469
36. Shubhanga KN, Anantholla Y (2006) Manual for a multi-machine small-signal stability programme. Dept. of Electrical Eng. NITK, Surathkal
37. Machowski J, Lubosny Z, Bialek JW, Bumby JR (2020) Power system dynamics: stability and control. Wiley, Hoboken
38. Pavella M, Murthy PG (1994) Transient stability of power systems: theory and practice.
39. Dey P, Mitra S, Bhattacharya A, Das P (2019) Comparative study of the effects of SVC and TCSC on the small signal stability of a power system with renewables. J Renew Sustain Energy 11(3):033305 **(pp 1–14)**
40. Mitra S, Bhattacharya A, Dey P (2018) Small signal stability analysis in co-ordination with PSS, TCSC, and SVC. In: 2018 International Conference on Computation of Power, Energy, Information and Communication (ICCPEIC) (pp 434–441). IEEE.
41. Dey P, Bhattacharya A, Datta J, Das P (2017) Small signal stability improvement of large interconnected power systems using power system stabilizer. In: 2017 2nd International Conference for Convergence in Technology (I2CT) (pp 753–760). IEEE.

42. Kashyap A (2015) Small-signal stability analysis and power system stabilizer design for grid-connected photovoltaic generation system (Doctoral dissertation, Carleton University).
43. Dey P, Bhattacharya A, Das P (2017) Tuning of power system stabilizer for small signal stability improvement of interconnected power system. Appl Comput Inf 1–14
44. Dey P, Bhattacharya A, Das P (2019) Tuned power system stabilizer for enhancing small signal stability of large interconnected power system. Caribbean J Sci 53(1):15 **(pp 843–857)**
45. Hauke B (2009) Basic calculation of a boost converter's power stage. Texas Instrum Appl Rep 1–9
46. Villalva MG, Gazoli JR, Ruppert Filho E (2009) Comprehensive approach to modeling and simulation of photovoltaic arrays. IEEE Trans Power Electron 24(5):1198–1208
47. Zhang Q, Wang R, Yang J, Ding K, Li Y, Hu J (2017) Collective decision optimization algorithm: a new heuristic optimization method. Neurocomputing 221:123–137
48. Saremi S, Mirjalili S, Lewis A (2017) Grasshopper optimisation algorithm: theory and application. Adv Eng Softw 105:30–47
49. Mirjalili S, Gandomi AH, Mirjalili SZ, Saremi S, Faris H, Mirjalili SM (2017) Salp Swarm Algorithm: a bio-inspired optimizer for engineering design problems. Adv Eng Softw 114:163–191



**Dr. Prasenjit Dey** completed his B.Tech in Electrical and Electronics Engineering from Anna University in 2010, M.Tech and Ph.D. in Power Systems from NIT Agartala in 2012 and 2020 respectively. His area of research deals with power system stability analysis. Presently he is working as an Assistant Professor in the Electrical and Electronics Engineering Department, NIT Sikkim, India.

**Dr. Anulekha Saha** completed her B.Tech in Electrical Engg. from West Bengal University of Technology in 2010, and M.Tech and Ph.D in Power Systems from NIT Agartala in 2012 and 2020 respectively. Her research area deals in power system optimization using soft-computing techniques. She has worked as an Assistant Professor in the Electrical Engineering Department, NIT Silchar, India, and is presently working as an Assistant Professor in the Electrical and Electronics Engineering Department, NIT Sikkim, India.

**Dr. Aniruddha Bhattacharya** did his B.Sc. in Electrical Engineering. from the Regional Institute of Technology, Jamshedpur, India, in 2000, and M.E.E. & Ph.D. in Electrical power system from Jadavpur University, Kolkata, India, in 2008 and 2011 respectively. His experience is diversified in industries as well as academics. He has worked with Siemens Metering Limited, India; Jindal Steel & Power Limited, Raigarh, India; Bankura Unnayani Institute of Engineering, Bankura, India; Dr. B. C. Roy Engineering College, Durgapur, India, NIT Agartala, India. Presently he is an Assistant Professor in the Electrical Engineering Department, NIT Durgapur, India. His areas of interest include power system load flow, optimal power flow, economic load dispatch, soft computing applications to power system problems.

**Dr. Boonruang Marungsri** was born in Nakhon Ratchasima Province, Thailand, in 1973. He received his B. Eng. and M. Eng. From Chulalongkorn University, Thailand in 1996 and 1999 and D. Eng. from Chubu University, Kasugai, Aichi, Japan in 2006, all in electrical engineering, respectively. Dr. Marungsri is currently an Asst. Prof. in the School of electrical engineering, Suranaree University of Technology, Thailand. His areas of interest are electrical power and Energy systems and high voltage insulation technologies.